Geoscientific
Model Development
Discussions

Impact of changes in climate and CO₂ on the carbon-sequestration potential of vegetation under limited water availability using SEIB-DGVM version 3.02

Shanlin Tong[1,2,3], Weiguang Wang[2,3*], Jie Chen[1 *], Chong-Yu Xu[4], Hisashi Sato[5], Guoqing Wang[6]

[1]State Key Laboratory of Water Resources and Hydropower Engineering Science, Wuhan University, Wuhan, 430072, Peoples R China

[2]State Key Laboratory of Hydrology-Water Resources and Hydraulic Engineering, Hohai University, Nanjing, 210098, Peoples R China

[3]College of Hydrology and Water Resources, Hohai University, Nanjing, 210098, Peoples R China

[4]Department of Geosciences, University of Oslo, Oslo, N-0316, Norway

[5]Japan Agency for Marine-Earth Science and Technology, Yokohama, 236-0001, Japan

[6]Nanjing Hydraulic Research Institute, Nanjing, 210029, Peoples R China

*Ccorrespondence to: Weiguang Wang (wangweiguang2016@126.com); Jie Chen (jiechen@whu.edu.cn)

Abstract

Documenting year-to-year variations in carbon-sequestration potential in terrestrial ecosystems is crucial for the determination of carbon dioxide (CO_2) emissions. However, the magnitude, pattern and inner biomass partitioning of carbon-sequestration potential, and the effect of the changes in climate and CO_2 on inner carbon stocks, remain poorly quantified. Herein, we use a spatially explicit individual based-dynamic global vegetation model to investigate the influences of the changes in climate and CO_2 on the enhanced carbon-sequestration potential of vegetation. The modelling included a series of factorial simulations using the CRU dataset from 1916 to 2015. The results show that CO_2 predominantly leads to a persistent and widespread increase in above-ground vegetation biomass carbon-stocks (AVBC) and below-ground vegetation biomass carbon-stocks (BVBC). Climate change appears to play a secondary role in carbon-sequestration potential. Importantly, with the mitigation of water stress, the magnitude of the above- and below-ground responses in vegetation carbon-stocks gradually increases, and the ratio between AVBC and BVBC increases to capture CO_2 and sunlight. Changes in the pattern of vegetation carbon storage was linked to regional limitations in water, which directly weakens and indirectly regulates the response of potential vegetation carbon-stocks to a changing environment. Our findings differ from previous modelling evaluations of vegetation that ignored inner carbon dynamics and

31 demonstrates that the long-term trend in increased vegetation biomass carbon-stocks is driven by CO_2

32 fertilization and temperature effects that are controlled by water limitations.

1 Introduction

34 As a result of the changes in climate and atmospheric carbon dioxide (CO_2), the terrestrial ecosystem

35 carbon cycle exhibits remarkable trends in interannual variations, which induce uncertainty in estimated

36 carbon budgets (Erb et al., 2018; Keenan et al., 2017). Recent studies assessing interannual fluctuations

37 in terrestrial carbon sinks have shown that the land carbon cycle is the most uncertain component of the

38 global carbon budget (Ahlstrom et al., 2015; Piao et al., 2020; Jung et al., 2017; Humphrey et al., 2018;

39 Gentine et al., 2019; Humphrey et al., 2021). These uncertainties result from an incomplete understanding

40 of vegetation biomass carbon production, allocation, storage, loss, and turnover time (Bloom et al., 2016).

41 The extent and distribution of vegetation carbon storage is central to our understanding of how to

42 maintain a balanced land carbon cycle. Changes in terrestrial vegetation carbon storage have a significant

43 effect on atmospheric CO_2 concentrations and determine whether biomes become a source or sink of

44 carbon (Erb et al., 2018; Humphrey et al., 2018; Terrer et al., 2021). Therefore, investigating the

45 processes producing changes in carbon storage is key to improving the accuracy of estimated terrestrial

46 carbon budgets, and to tap the greenhouse-gas moderation potentials of vegetation (Ipcc, 2007; Roy et

47 al., 2001).

49 The response of vegetation carbon storage to greenhouse effects results from two mechanisms, direct

50 effects of CO_2 on photosynthesis and indirect effects of changes in climate change and CO_2 on

51 photosynthesis, respiration, and sequestration (Schimel et al., 2015; Gentine et al., 2019; Cheng et al.,

52 2017). Since the beginning of industrialization, there has been a noticeable enhancement in the capacity

53 of sequestering carbon, which is needed for stabilizing greenhouse gas concentrations (Chen et al., 2019;

54 Pan et al., 2011; Le Noë et al., 2020; Magerl et al., 2019; Bayer et al., 2015; Harper et al., 2018). This

55 increase has coincided with a widespread change in other vegetation features, including a positive

56 increase in annual gross primary productivity and a greening of the biosphere (Madani et al., 2020; Zhu

57 et al., 2016). The spatiotemporal distribution and environmental drivers in carbon-sequestration potential

58 have been well documented on the basis of model estimates and satellite-based assessments (Erb et al.,

59   2007; Erb et al., 2018; Bazilevich et al., 1971; Saugier et al., 2001; Bartholome and Belward, 2005; Olson

60   et al., 1983; Pan et al., 2013; Ajtay et al., 1979; Ruesch and Gibbs, 2008; Kaplan et al., 2011; Shevliakova

61   et al., 2009; Prentice et al., 2011; West et al., 2010; Hurtt et al., 2011). In contrast, the variability of

62   above- and below-ground partitioning of carbon-sequestration potential has not been extensively studied.

63   Without an accurate assessment of the dynamics of each fraction, attribution of carbon-sequestration

64   potential to environmental drivers is highly uncertain. Consequently, partitioning potential vegetation

65   carbon storage and revealing its inner processes are essential to accurately comprehend the current state

66   of carbon sequestration capacity and predict how it will change in the future, both of which are key

67   instruments in revealing the influence of various drivers on the enhancement of carbon-sequestration

68   potential.

69

70   The variability in vegetation carbon flux is also linked to terrestrial water availability (Gentine et al.,

71   2019; Seo and Kim, 2019). Thus, potential water limitations impart another constraint on the global

72   ecosystem carbon cycle. Typically, increasing water stress limits the response magnitude of carbon

73   uptake rates through a down-regulation of stomatal conductance (Humphrey et al., 2021). Trees and herbs

74   are tuned to allocate higher carbon-flux to roots when mitigating for the adverse effects of limited water

75   availability (Friedlingstein et al., 1999). Water availability controls both carbon allocation and storage

76   and can potentially transform regions characterized by a negative response to climate to regions

77   exhibiting a positive response. For example, warming has a negative effect on the percentage of roots in

78   dry regions and increases the ratio of above- versus belowground biomass in wet regions (Ma et al.,

79   2021). This is particularly apparent in tropical regions, where variations in water availability can result

80   in different responses in the processes involved in the carbon cycle (Liu et al., 2017). The differences in

81   the response mechanisms influencing the vegetation carbon flux among different hydrological regions is

82   related to plant oversensitivity to hydrological gradients. Thus, it is important to systematically

83   investigate the distinct responses of carbon-sequestration potential to changes in climate and CO_2 under

84   differing conditions of water stress.

85

86   As documented above, many studies have investigated the integral changes in regional and global

87   terrestrial storage of carbon, while few studies have examined trends in the partitioning of carbon storage

88   by vegetation biomass. Large gaps in our knowledge of the effects of various drivers on the partitioning

89   of carbon-stocks in vegetation biomass remain. Importantly, an increase in the magnitude of water stress

90   may dramatically change the impact of these drivers on above- versus below-ground partitioning of

91   carbon-sequestration potential (Ma et al., 2021). Evaluating the response pattern of carbon-stocks to

92   various drivers under conditions of limited water is elemental for clearly documenting the response

93   mechanism of vegetation carbon-sequestration potential.

94

95   Here, we use a spatially explicit individual-based dynamic global vegetation model (SEIB-DGVM),

96   along with the root-shoot ratio method (R/S) to (1) systematically determine the long-term variability of

97   carbon-sequestration potential and understand its response mechanisms, and (2) estimate trends in

98   partitioning of potential biomass carbon-stocks of vegetation biomass. Throughout this study, the

99   potential biomass carbon-stock is recognized as a proxy for the potential of carbon-sequestration by

100 natural vegetation. Using a set of factorial simulations to isolate responses to environmental change, we

101 analyse the contributions of multiple driving factors to the trends of two fractions of carbon-stocks at

102 large scales individually. We then conceptualize the role of water availability through an aridity index

103 (AI), in which hydrological regions are subdivided by their degree of aridity. By comparing the

104 differences in the magnitude of response between the fractions of above- and belowground carbon-stocks

105 for varying degrees of water availability, we assess the effect of water limitations on the response pattern

106 of potential carbon-stocks to changes in climate and CO_2.

107 **2 Model description, experimental design, observational data, and evaluation metrics**

108 In this section, we provided a list of data source (Sect. 2.1), an overview of the modelling concept (Sect.

109 2.2), the representation of biomass carbon-stock partitioning in the SEIB-DGVM (Sect. 2.3), an overview

110 of the experimental scheme used in the model simulations (Sect. 2.4), and the validation of model results

111 (Sect. 2.5).

112 **2.1 Forcing Data**

113 Long-term daily meteorological time-series data are required to run model simulations, including

114 precipitation, daily range of air temperature, mean daily air temperature, downward shortwave radiation,

115 downward longwave radiation, wind velocity and relative humidity. These data were obtained from the

116 Climatic Research Unit (CRU) time series 4.00 gridded dataset (degree 0.5°) for the period 1901–2015

117 (Harris et al., 2020). Because the CRU dataset is a monthly based dataset, the monthly meteorological

118 data were converted into daily climatic variables by supplementing daily climatic variability within each

119 month using the National Centre for Environmental Prediction (NCEP) daily climate dataset. The NCEP

120 data, displayed using the T62 Gaussian grid with 192×94 points, was interpolated into a 0.5° grid (which

121 corresponds to the CRU dataset) using a linearly interpolation method. By combining the CRU data, with

122 the interpolated NCEP dataset, we were able to directly obtain the most of driving meteorological data

123 (details in Sato et al. (2020)). Neither the CRU nor NCEP datasets included downward shortwave and

124 longwave radiation. Thus, daily cloudiness values in the NCEP were used to calculate radiation values

125 using empirical functions (Sato et al., 2007). These data were all aggregated to a daily timescale with 0.5°

126 resolution to run SEIB-DGVM.

127

128 Atmospheric CO_2 concentrations were collected from Sato et al. (2020), which contains reconstructed

129 CO_2 concentrations between 1901 and 2015. The statistical reconstruction of global atmospheric CO_2

130 was used in this analysis. These reconstructions were based on present annual CO_2 concentrations

131 recorded from the Mauna Loa monitoring station. These data assume atmospheric CO_2 concentration

132 was 284 ppm in 1750, and statistically interpolates atmospheric CO_2 concentrations to fill the gap from

133 1750 to 2015.

134

135 The physical parameters of the soil used in the model include soil moisture at the saturation point, field

136 capacity, matrix potential, wilting point and albedo. These data were obtained from the Global Soil

137 Wetness Project 2.

138 **2.2 Overview of modelling concept in SEIB-DGVM**

139 Model SEIB-DGVM version 3.02 (Sato et al., 2020) was employed in this study. This is a process-based

140 dynamic global vegetation model driven by meteorological and soil data. It is an explicit and

141 computationally efficient carbon cycle model designed to simulate transient effects of environmental

142 change on terrestrial ecosystems and land-atmosphere interactions. It describes three groups of processes:

143 land-based physical processes (e.g., hydrology, radiation, aridity), plant physiological processes (e.g.,

144   photosynthesis, respiration, litter), and plant dynamic processes (e.g., establishment, growth, mortality).

145   Twelve plant functional types (PFTs) were classified. During the simulation, a sample plot was

146   established at each grid box, and then the growth, competition, and mortality of each the individual PFTs

147   within each plot were modelled by considering the specify conditions for that individual as it relates to

148   other individuals that surround it (Sato et al., 2007).

149

150   SEIB-DGVM treats the relationships between soil, atmosphere, and terrestrial biomes in a consistent

151   manner, including the fluxes of energy, water, and carbon. Based on specified climatic conditions and

152   soil properties, SEIB-DGVM simulates the carbon cycle, energy balance, and hydrological processes.

153   SEIB-DGVM utilizes three computational time steps: (1) a daily time step for all physical and

154   physiological processes, including soil decomposition and tree growth, (2) a monthly time step for tree

155   growth, and (3) an annual time step for tree establishment and death. The simulated unit of the model is

156   a 30 m × 30 m spatially explicit 'virtual forest'. A grass layer was placed under the woody layer, and

157   provides for a comprehensive, spatially explicit quantification of terrestrial carbon sinks and sources.

158   The soil depth was set at 2 m and was divided into 20 layers, each with a thickness of 0.1 m. The

159   photosynthetic rate of a single-leaf was simulated following a Michaelis-type function (Ryan, 1991).

160   Respiration was divided into two types: growth respiration and maintenance respiration. Growth

161   respiration is defined as a construction cost for plant biosynthesis, which is quantified by the chemical

162   composition of each organ (Poorter, 1994). Maintenance respiration of live plants occurs every day

163   regardless of the phenological phase, and is controlled by the temperature and nitrate content of each

164   organ (Ryan, 1991). Atmospheric CO_2 was envisioned to be absorbed by photosynthesis of woody PFTs

165   and grass PFTs. This assimilated carbon flux was then allocated into all the plant organs (leaf, trunk, root,

166   and stock), where maintenance respiration and growth respiration occur. The hydrology module treats

167   precipitation, canopy interception, transpiration, evaporation, meltwater, and penetration.

168

169   SEIB-DGVM differs from other dynamic global vegetation models in that it is a biogeochemical model

170   that represents plant structure in three-dimensions. This representation of vegetation dynamics has two

171   advantages. First, it directly uses *in-situ* data about PFT dynamics and structure as tuning or validation

172   data, without adding additional assumptions. Second, sunlight and other resources are distributed among

Geoscientific
Model Development
Discussions

173   individuals without human disturbances, leading to a more properly calculated and accurate

174   representation of the responses of potential vegetation biomass to external environmental change.

175   Therefore, SEIB-DGVM, in general, effectively represents plant competition and function dynamics

176   under environmental change (Sato et al., 2007).

177   **2.3 Carbon-stock of vegetation biomass partitioning**

178   **2.3.1 Parameterization of daily allocation**

179   Flexible allocation schemes about resources and biomass are set up in the framework of the SEIB-DGVM

180   biogeochemical model. Atmospheric CO_2 is assimilated by the photosynthesis of both woody and grass

181   foliage, and then is added into the non-structural carbon of the plant. This non-structural carbon of

182   photosynthetic production is allocated to all the plant organs (foliage, trunk, root, and stock), supplying

183   what is needed for the maintenance and growth of each organ. When the non-structural carbon is greater

184   than 0 during the growth phase, the following dynamic carbon allocation is executed for each individual

185   plant at the daily time scale, such that:

186   (1) When the fine root biomass ($mass_{root}$) of wood or grass does not satisfy minimum requirements for

187   fulfilling functional balance ($mass_{leaf}$/FR_{ratio}), the mass of non-structural carbon is allocated to the root

188   biomass to supplement the deficit. Here, $mass_{leaf}$ is the leaf biomass, and FR_{ratio} is the ratio of $mass_{leaf}$ to

189    $mass_{root}$ satisfying the functional balance.

190   (2) The stock biomass is supplemented until it is equal to leaf biomass. This scheme is active after the

191   first thirty days of the growing phase.

192   (3) Woody leaf biomass is constrained by three limitations of the maximum leaf biomass, which are

193   calculated as follows:

$$max_1 = \left(crown_{area} + \pi crown_{diameter} crown_{depth}\right)\frac{LA_{max}}{SLA} \qquad (1)$$

$$max_2 = ALM_1 \frac{\pi(dbh_{heartwood}/2 + dbh_{sapwood}/2)^2 - \pi(dbg_{heartwood}/2)^2}{SLA} \qquad (2)$$

$$max_3 = \frac{mass_{available}}{RG_f} \qquad (3)$$

$$mass_{leaf} = \min(max_1, max_2, max_3) \qquad (4)$$

198   where max_1, max_2, and max_3 are, respectively, maximum leaf biomass for a given crown surface area,

199   cross-sectional area of sapwood, and non-structural carbon, SLA is a constant of PFTs leaf area (m^2 g^{-1}),

200   LA_{max} is maximum leaf area of PFTs per unit biomass (m^2 m^{-2}), and ALM_1 represents the area of

201   transport tissue per unit biomass, and is a constant (dimensionless). If the mass$_{leaf}$ is less than the

202   minimum (max_1, max_2, max_3), the mass of non-structural carbon is allocated into leaf biomass to

203   supplement the deficit.

204   Grass leaf biomass is supplemented until the leaf area index of grass equals the optimal leaf area index,

205   which are calculated as:

206   $$lai_{opt} = \frac{\ln par_{grass} - \ln\left\{\frac{p_{sat}}{lue}\left[\left(1 - \frac{cost/SLA}{0.09093 \times dlen \times p_{sat}}\right)^{-2} - 1\right]\right\}}{eK} \tag{5}$$

207   where lai_{opt} is optimal leaf area index (m^2 m^{-2}), par_{grass} is the grass photosynthetically active radiation

208   (μmol photon m^{-2} s^{-1}), p_{sat} is the light-saturated photosynthetic rate (μCO$_2$ m^{-2} s^{-1}), lue is the light-use

209   efficiency of photosynthesis (mol CO$_2$ mol photon^{-1}), $cost$ is the cost of maintaining leaves per unit leaf

210   mass per day (g DM g DM^{-1} day^{-1}), $dlen$ is day length (hour), and eK is light attenuation coefficient at

211   midday.

212   (4) When non-structural carbon is less than 10 g dry mass (DM) PFT^{-1} or annual NPP is less than 10 g

213   DM PFT^{-1} in the previous year, the following daily simulation processes (5~6) will be skipped.

214   (5) When total woody biomass is more than 10 kg DM, which defines the minimum tree size for

215   reproduction, 10% of non-structural carbon is transformed into litter.

216   (6) During the simulation of trunk growth, the remaining structural carbon is allocated to sapwood

217   biomass. There is no direct allocation to heartwood, which is transformed slowly from sapwood biomass.

218   For grass PFTs biomass, the densities of all organs comprising the biomass never decline below 0.1 g

219   DM m^{-2} even if the environment is deteriorated for grass survival. A more detailed description of SEIB-

220   DGVM is given by Sato et al. (2007).

221

222   Terrestrial water availability represents a significant source of variability in the ecosystem carbon cycle

223   (Humphrey et al., 2021; Humphrey et al., 2018; Ma et al., 2021). To control plant phenology and the rate

224   of photosynthesis as a function of the limitation in terrestrial water, the physiological status of the

225   limitation of terrestrial water is calculated as:

226   $$stat_{water} = \frac{max(pool_{w(1)}/Depth_{(1)}, \; pool_{w(2)}/Depth_{(2)}) - W_{wilt}}{W_{fi} - W_{wilt}} \tag{6}$$

227   where $stat_{water}$ is the physiological status of the terrestrial water limitation, which ranges between 0.0–

228   1.0, dimensionless, $pool_{w(n)}$ is the water content in soil layer n, mm, $Depth_{(n)}$ is depth of the soil layer

229   n, mm, W_{wilt} is soil moisture at the wilting point, m m^{-1}, and W_{fi} is soil moisture at field capacity, m

230   m^{-1}. When the temperature of all soil layers is less than 0°C, $stat_{water}$ is equal to 0.

231   **2.3.2 Carbon-stock partitioning method**

232   According to the flexible allocation scheme, SEIB-DGVM allocates and stores the biomass carbon in

233   four pools of woody PFT (foliage, trunk, root, and stock) and three pools of grass PFT (foliage, root, and

234   stock). To investigate the fractional variability of carbon-sequestration potential between the pools, we

235   partitioned potential vegetation carbon-stocks based on the physiological function of the plant (Figure

236   A1). The root-shoot ratio (R/S) has been widely used to investigate the relationship between aboveground

237   vegetation biomass to belowground vegetation biomass and is considered an important variable in the

238   terrestrial ecosystem carbon cycle (Zhang et al., 2016). In this study, we adjusted the method of

239   calculating the R/S ratio by distinguishing between the aboveground vegetation biomass carbon-stock

240   (AVBC) and the belowground vegetation biomass carbon-stock (BVBC). AVBC includes biomass carbon

241   from woody foliage, woody trunk, and grass foliage, while BVBC includes biomass carbon from woody

242   fine roots and grass fine roots, excluding the stock pool. Thus,

243     $\frac{AVBC}{BVBC} = \frac{Wmass_{leaf}+Wmass_{trunk}+Gmass_{leaf}}{Wmass_{root}+Gmass_{root}} \times 100\%$ (7)

244   where $AVBC$ is aboveground vegetation biomass carbon-stock (kg C m^{-2}), $BVBC$ is belowground

245   vegetation biomass carbon-stock (kg C m^{-2}), $Wmass_{leaf}$ is the leaf biomass carbon-stock of wood (kg

246   C m^{-2}), and $Wmass_{trunk}$ is the trunk biomass carbon-stock of wood (kg C m^{-2}), including both branch

247   and structural roots. This biomass is simplistically attributed to aboveground organs and is used primarily

248   to support the plant. $Gmass_{leaf}$ is the leaf biomass carbon-stock of grass (kg C m^{-2}), whereas

249     $Wmass_{root}$ and $Gmass_{root}$ are functional root (fine roots) biomass carbon-stocks of wood and grass,

250   separately (kg C m^{-2}), which absorb water and nutrition from soil.

251   **2.4 Experimental design**

252   **2.4.1 Setup of model runs**

253   SEIB-DGVM simulations begin with seeds of selected plant function types planted in bare ground. The

254   plant functional types are favored for establishment by the environmental conditions in each grid cell.

255   We inputted the transient climate data from 1901 to 1915 to spin up the model in a repetitive loop. No

256 obvious trend in climatic factors was observed during this period (Tei et al., 2017). A spin-up period of

257 1050 years was necessary to bring the terrestrial vegetation carbon cycle into a dynamic equilibrium. To

258 reach quasi-equilibrium in the vegetation biomass, about 1000 years of simulation was required as a spin-

259 up procedure.

260 **2.4.2 Factorial simulation scheme**

Table 1. List of factorial simulations used in this study

Factorial simulation	CO_2 fertilization	Precipitation	Temperature	Radiation	Other drivers
S1	√	√	√	√	√
S2	√				
S3	√	√			
S4	√		√		
S5	√			√	
S6	√				√

Note: In factorial simulation S1, historical atmospheric CO_2 concentration and historical climate fields from the CRU data set were used. In simulation S2, only historical atmospheric CO_2 concentration was used, and climate variables of the transient period (1901–1915) were repeatedly input. In simulation S3 (or S4, S5), only historical atmospheric CO_2 concentrations and precipitation (or temperature, radiation) were input, and climate variables of the transient period (1901–1915) were repeatedly input. In the last simulation S6, historical atmospheric CO_2 concentrations and other climate variables were input, excluding precipitation, temperature, and radiation.

261 To further quantify the relative contributions of varying atmospheric CO_2 concentrations, precipitation,

262 temperature, and radiation, we performed six factorial simulations after the spin-up procedure using

263 different input variables between 1916 and 2015 (Table 1). Other drivers included wind velocity and

264 relative humidity. Consistent with previous studies (Zhu et al., 2016; Piao et al., 2006), the contribution

265 of CO_2 to the trend in carbon-stocks trend was defined as the ratio of the carbon-stock increase from

266 simulation S2 to that of simulation S1. The contributions of precipitation, temperature, radiation, and

267 other factors were calculated by subtracting simulation S2 from each corresponding simulation (S3, S4,

268 S5, S6, respectively), then dividing by simulation S1.

269 **2.4.3 Non-parametric test methods**

270 Each driving factor (atmosphere CO_2, precipitation, temperature, and radiation) has a different influence

271 on the carbon-stock, so it is difficult to make a simple pre-assumption about the population distribution

272 pattern for factorial simulations. We used the non-parametric Mann-Kendall and Sen's slope estimator

273 statistical tests (Gocic and Trajkovic, 2013) to assess the ability of SEIB-DGVM to simulate the response

274   patterns of carbon-sequestration potential to a change in climate and CO_2 concentrations. We regressed

275   the simulated hundred-year mean global average carbon-stock time series to reveal the accumulative

276   influences of the single variables based on the factorial simulations where only one or two drivers were

277   varied. Detection trends of AVBC and BVBC for all driving factors performed statistically well (in

278   agreement at the 95% confidence intervals), indicating this analytical method was suitable for trend

279   attribution at the global scale.

280   **2.4.4 Distinguishing hydrological regions**
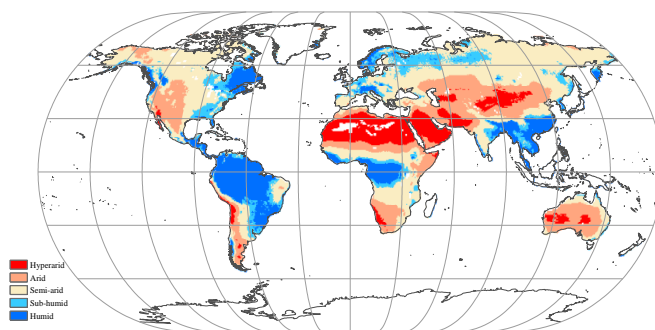
Figure 1. Global spatial patterns of water availability. Spatial variations in water availability were categorized based on an 115-year average aridity index (AI), defined as the ratio of the multiyear mean precipitation to the potential evapotranspiration. Categories include: hyper-arid (AI ≤ 0.05), arid (0.05 < AI ≤ 0.2), semi-arid (0.2 < AI ≤ 0.5), sub-humid (0.5 < AI ≤ 0.65), and humid (AI > 0.65).

281   Locally available water strongly regulates and limits the response of carbon-stocks to changes in climate

282   and CO_2. We defined an aridity index (AI) to distinguish between the global hydrological regions for

283   comparing the long-term trend in carbon-stocks over different hydrological environments, and for

284   quantifying the influences of each hydrological environment on the variations in the trends. The AI was

285   defined as:

286     $AI = \dfrac{\bar{P}}{\overline{ET_p}}$ (8)

287   where $\bar{P}$ is the multiyear mean precipitation (mm year^{-1}), and $\overline{ET_p}$ is the multiyear mean potential

288   evapotranspiration (mm year^{-1}), which was calculated by the Penman-Monteith model (Monteith and

289   Unsworth, 1990). As in a previous study (Chen et al., 2019), five hydrological regions (Figure 1) were

290   categorized based on an 115-year average AI (1901–2015): including a hyper-arid region (AI ≤ 0.05),

291   arid region (0.05 < AI ≤ 0.2), semi-arid region (0.2 < AI ≤ 0.5), sub-humid region (0.5 < AI ≤ 0.65), and

292   humid region (AI > 0.65).

3 Results and discussion

3.1 Evaluation of SEIB-DGVM

295   In terrestrial vegetation biomes, there is a high correlation between biomass carbon-stock density and

296   NPP per unit (Erb et al., 2016; Kindermann et al., 2008) (Figure A1). Thus, we initially used NPP as a

297   proxy of the carbon-stock to assess model accuracy. We obtained the dataset from the Ecosystem Model-

298   Data Intercomparison (EMDI) working group, and then compared their data with modelled multiyear

299   average NPP in the period of 1916-1999. The EMDI dataset is an ensemble from global ecological sites

300   from 1901 to 1999 and is shown in Figure 2. The determined coefficient (R^2) between EMDI observed

301   and estimated multiyear average NPP of 669 *in-situ* observations is 0.54, which is significant at the

302   p=0.01 level. The slope of the regressed line is 0.70 during the twentieth century.

(a)

Multiyear average NPP simulated by SEIB-DGVM (gC m^{-2} yr^{-1})

50   100   200   300   400   500   600   700   800   900   1000   1100   1200   1500

(b)

Y=0.6979X+178.68
R^2=0.54
P<0.01
N=669
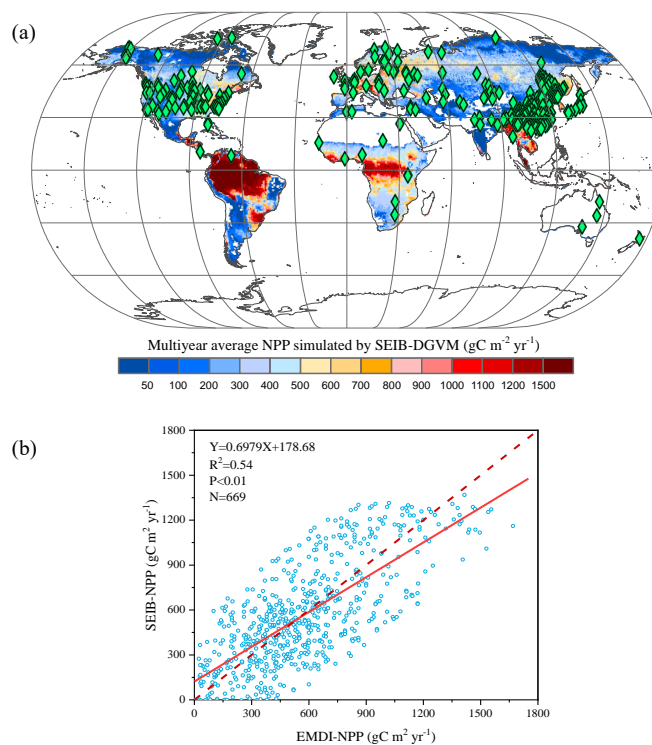
Figure 2. Multiyear average NPP calculated by SEIB-DGVM and EMDI for the twentieth century. (a) EMDI global site distribution. Green rhombuses indicate the locations of the sites. (b)

Comparison of NPP calculated by SEIB-DGVM and EMDI. The solid line is the best fit curve; and the dashed line represents a perfect correspondence in the results of the two.

303 However, *in-situ* observations are sparse for global spatial-temporal validation. Therefore, we used the

304 MOD17A3 products to further verify the simulated potential NPP from 2000 to 2015. These data were

305 collected by the Moderate Resolution Imaging Spectroradiometer and are some of the most widely used

306 data to assess the accuracy of global model simulations (Gulbeyaz et al., 2018). The potential vegetation

307 refers to the hypothetical condition that would prevail in an assumed absence of anthropogenic activity,

308 but under historical climate fields (Erb et al., 2018; Haberl et al., 2014). The potential NPP in the potential

309 vegetation is defined as that the assimilated carbon stored in land vegetation without human disturbance

310 under current environmental conditions (Erb et al., 2018). We resampled actual NPP data from

311 MOD17A3 to a common spatial resolution (0.5°) by the majority method. Potential NPP-MOD17A3

312 data were extracted from typical NPP values in grids only covered by vegetation from actual NPP-

313 MOD17A3 data. Regions covered by undisturbed vegetation were distinguished from a land vegetation

314 cover map. Figure 3 shows that the modelled NPP from the SEIB-DGVM exhibited a high degree of

315 consistency with the NPP-MOD17A3 data over the period (R^2=0.62, $p<0.05$). The general

316 spatiotemporal agreement between the simulated NPP derived from SEIB-DGVM with *in-situ*

317 observations and derived from satellites reveals that it is reasonable to use the SEIB-DGVM simulations

318 to evaluate the same mechanisms controlling global potential biomass carbon stocks of vegetation.
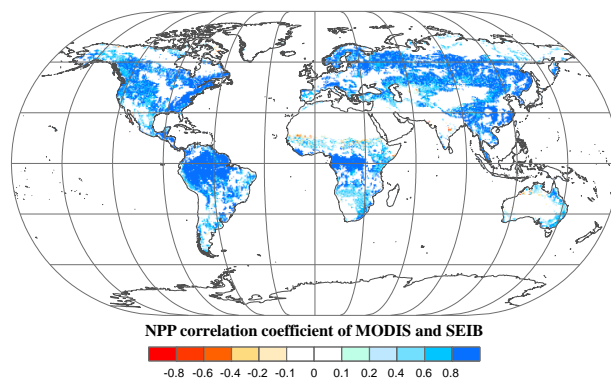

NPP correlation coefficient of MODIS and SEIB

-0.8 -0.6 -0.4 -0.2 -0.1 0 0.1 0.2 0.4 0.6 0.8

Figure 3. Spatial patterns in the potential NPP correlation coefficients between SEIB-DGVM and MODIS between 2001–2015. These data were used to validate SEIB-DGVM.

319 For obtaining potential NPP-MOD17A3 data, we collected a land-use dataset from MCD12C1 to make

320 a vegetation cover map in the period of 2001–2015. We resampled the land cover map to a common

Geoscientific
Model Development
Discussions

321   spatial resolution (0.5°), and extracted grids of covered vegetation to produce the land vegetation cover

322   map (Figure A2). Cover types on the map include evergreen needleleaf forests, evergreen broadleaf

323   forests, deciduous needleleaf forests, deciduous broadleaf forests, mixed forests, closed shrublands, open

324   shrublands, woody savannas and grasslands.

325

326   Finally, the modelled result of potential vegetation biomass carbon-stock was compared with current

327   existing data form the literature and state-of-the-art datasets. Figure 4 shows that the modelled results are

328   within the range of potential carbon-stocks, which indicate that the SEIB-DGVM reliably simulated the

329   carbon-stock dynamics.
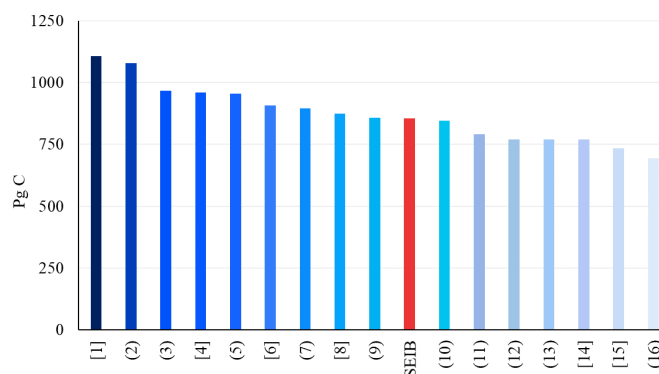
Figure 4. Estimates of the potential vegetation biomass carbon-stock from the literature (parentheses), state-of-the-art datasets (brackets) and this study. Datasets are from the following studies: [1](Erb et al., 2018; Erb et al., 2007), (2)(Bazilevich et al., 1971), (3)(Saugier et al., 2001), [4](Erb et al., 2018; Bartholome and Belward, 2005), (5)(Olson et al., 1983), [6](Erb et al., 2018; Pan et al., 2011), (7)(Ajtay et al., 1979), [8](Erb et al., 2018; Ruesch and Gibbs, 2008), (9)(Kaplan et al., 2011), (10)(Shevliakova et al., 2009), (11)(Kaplan et al., 2011), (12)(Pan et al., 2013), (13)(Prentice et al., 2011), [14](Erb et al., 2018; Erb et al., 2007), [15](Erb et al., 2018; West et al., 2010), (16)(Hurtt et al., 2011). The red column is the SEIB-DGVM-modelled biomass carbon stocks used in this study.

330   **3.2 Enhanced carbon-stocks and its fractions**

331   A global time series of potential vegetation carbon-stocks and its partitioning fractions were modelled by

332   the SEIB-DGVM between 1916–2015. The simulations were conducted at a spatial resolution of 0.5°

333   and at a daily timescale using CRU and reconstructed atmospheric CO_2 concentration data. We

334   distinguished the changes of AVBC and BVBC from integral vegetation carbon-stocks. The historical

335   temporal trends over the period are shown in Figure 5a. The potential vegetation carbon-stock (the year-

336 to-year accumulation of carbon in the terrestrial plant without external interference) exhibits a net

337 increase of 119.26 ± 2.44 Pg C in the last century (± 2.44 represents monthly fluctuation in carbon within

338 the year). This increasing trend exhibits a robust agreement with the slower increase in atmospheric CO_2

339 concentration ($R^2=0.88$, $p<0.001$), suggesting that the carbon-stock is strongly affected by CO_2

340 fertilization. In addition, the positive correlation between the carbon-stock and CO_2 generally extends

341 across all vegetation biomass partitions (AVBC+BVBC). After the value of the global terrestrial carbon-

342 stock and trends were partitioned among the vegetation functional classes, we see that AVBC increases

343 116.18 ± 2.34 Pg C (or ~15.60%) and dominates the positive global carbon-stock trend; BVBC also

344 increases 3.08 ± 0.14 Pg C (or ~18.03%) over the past century.
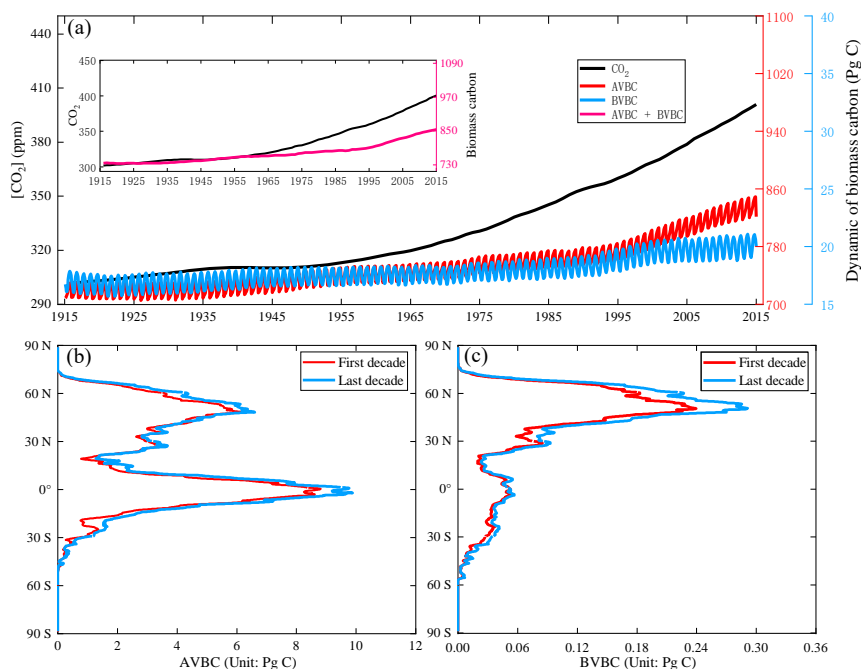
Figure 5. Global potential biomass carbon stocks of vegetation during the past 100 years. (a) The
evolution of global potential biomass stocks (AVBC+BVBC), along with changes in biomass stocks
that can be attributed to the variability and trend of AVBC and BVBC through the twentieth century.
The red line represents the monthly value of AVBC, the blue line represents the monthly value of
BVBC, and the pink line represents the annual value of potential vegetation carbon stock. **(b, c)** Zonal
averaged sums of the annual AVBC and BVBC for latitudinal bands during the first decade; the
averaged value (1916–1925, red line) and the last decade averaged value (2006–2015, blue line) shows
the increased carbon stock capacity.

345 The global distributions of the decadal-average change in AVBC and BVBC are shown in Figures 5b and

346 5c, respectively. The significant historical changes in climate and CO_2 enhance the carbon-stock of the

347 terrestrial ecosystem, and their positive influences are broadly distributed across a latitudinal north–south

348 gradient. The latitudinal bands of increasing annual AVBC are mainly distributed in the tropic and boreal

349 latitudes, a conclusion consistent with prior knowledge (Erb et al., 2018; Schimel et al., 2015). The

350 decadal and inter-annual variabilities of AVBC are dominated by the tropical and semi-arid regions where

351 large portions of the regions are highly productive (Ahlstrom et al., 2015; Poulter et al., 2014). There is

352 a single peak in the spatial variation of annual BVBC (Figure 5c). BVBC exhibits robust growth at most

353 latitudes, and it increases mainly in boreal latitudes.

354 **3.3 Spatial variability in estimated AVBC and BVBC trends**

355 Based on the carbon-stock partitioning method, we found that the integrated carbon-stock as well as the

356 above- and belowground carbon-stocks over the period of 1916–2015 exhibited a remarkable spatial

357 heterogeneity. Figure 6a shows that an increase in vegetation carbon-stocks occurred over regions and

358 global aggregate levels during the entire study period. About 57.39% of the terrestrial grids exhibited an

359 increase with a noticeable trend (p<0.05) in biomass carbon-stock; 53.82% of global grids possessed

360 increases that were statistically significant at the p=0.01 level. To determine the contributions of each

361 fraction (AVBC, BVBC) to the integral change in the potential vegetation carbon-stock, we partitioned

362 and present the historical spatial and temporal patterns for each fraction separately (Figure 6b, 6c). AVBC

363 contributes 97.33% to the total incremental change (116.18 ± 2.34 Pg C), with about 51.32% of the grids

364 possessing a noticeable positive trend (p=0.01). Generally, spatial patterns of AVBC and the integral

365 carbon-stock are consistent (Figure 6a, 6b), which further supports the argument that AVBC dominates

366 the trend in carbon-stocks in most regions. Although the proportion of the total change in carbon-stocks

367 is small (3.08 ± 0.14 Pg C), about 61.00% of the land surface shows an increase in BVBC; of these

368 terrestrial grids, 55.81% was characterized by a significant p=0.01 increase.
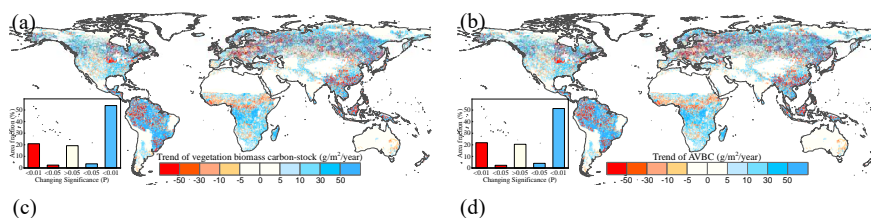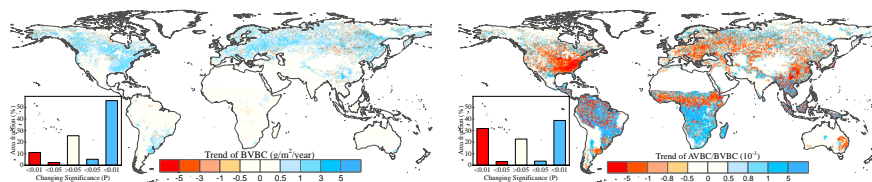
Figure 6. Spatial patterns in the trends of potential vegetation carbon-stocks and their fractions from 1916 to 2015. Difference induced by changes in climate and CO_2 in terrestrial biomass carbon-stock (a), AVBC (b), and BVBC (c) during the historic period 1916–2015. (d) Trend in the AVBC/BVBC ratio from 1916 to 2015. The sub-graphs show the significant test results. The white bar indicates non-vegetated areas, or the trend is statistically insignificant (P >0.05). The blue bar indicates significantly increasing trends in the ratio and vice versa.

369   Biomass carbon allocation between above- and belowground vegetation organs reflect the changes in

370   individual growth, community structure and ecosystem function, which are important attributes in the

371   investigation of carbon-stocks and carbon cycling within the terrestrial biosphere (Hovenden et al., 2014;

372   Fang et al., 2010; Ma et al., 2021). Under the influences of a changing climate and CO_2 concentrations,

373   there is a slight increase in the ratio of global AVBC/BVBC; the rate of increase is 0.0171 yr^{-1} in the last

374   hundred years, which is significant at the 0.01 level (Figure 6d). Regions with noticeable increases in the

375   ratio of AVBC to BVBC are mainly located in southern Africa, central South America, and northern

376   Eurasia. Negative trends in AVBC/BVBC ratios are found in northern America, southern Europe, and

377   tropical Africa.

378   **3.4 Responses of AVBC and BVBC to environmental drivers**

379   The responses of AVBC and BVBC to changes in climate and CO_2 are both positive at the global level

380   (Figure 7a, 7c), although regionally, they exhibit both negative and positive responses (Figure 7b, 7d).

381   Based on the results of factorial simulations and Mann-Kendall+Sen tests, CO_2 fertilization explains the

382   largest proportion of the change in the carbon-stock, about 82.45% change in AVBC was positive (15.521

383   g C m^{-2} yr^{-1}), whereas 89.28% of the change in BVBC was positive (0.435 g C m^{-2} yr^{-1}). The separately

384   simulated AVBC and BVBC increased by 80.98 Pg C and 2.66 Pg C with increasing atmospheric CO_2

385   concentrations (from 301.73 ppm in 1916 to 400.83 ppm in 2015). The other climatic drivers

386   (precipitation, temperature, radiation, humidity, and wind speed) remained at baseline values. While the

387   increase or decrease in the carbon-stock may be attributed to more than one driving factor, within any

388   specified grid, the one with the highest contribution was the driver that consistently resulted in the highest

389 increase or decrease in the carbon-stock for that grid. The spatial pattern illustrates that CO_2 dominates

390 the variability in AVBC in 7.28% of the regions, including 1.21% of the regions that exhibited a negative

391 change and 6.07% that exhibited a positive change. CO_2 dominates the variability in BVBC in 27.60%

392 of the regions, including 1.73% of the regions that exhibited a negative change and 25.87% of regions

393 with a positive change (Figure 7b, 7d). These trends are consistent with previous studies (Tharammal et

394 al., 2019; Zhu et al., 2016; Keenan et al., 2017) in which positive trends occurred, especially for BVBC.

395 The responses of terrestrial ecosystems to high CO_2 concentration are affected by vegetation species and

396 the dynamic function of the vegetation carbon-stock. Due to the interaction between terrestrial vegetation

397 and a changing environment, both photosynthesis and respiration of the vegetation also changed. To

398 better absorb CO_2 and sunlight required for photosynthesis, vegetated regions are gradually covered by

399 vegetation with higher plant height and wider leaf area, thereby adjusting their characteristic ecosystem

400 functions (Anderson et al., 2010) (Figure 6d). Fractional dynamics of the carbon-stock (AVBC/BVBC)

401 are widely used as a key indicator to investigate the responses of vegetation to environmental drivers,

402 which also reflect the response strategies of vegetation in environments with different water limitations
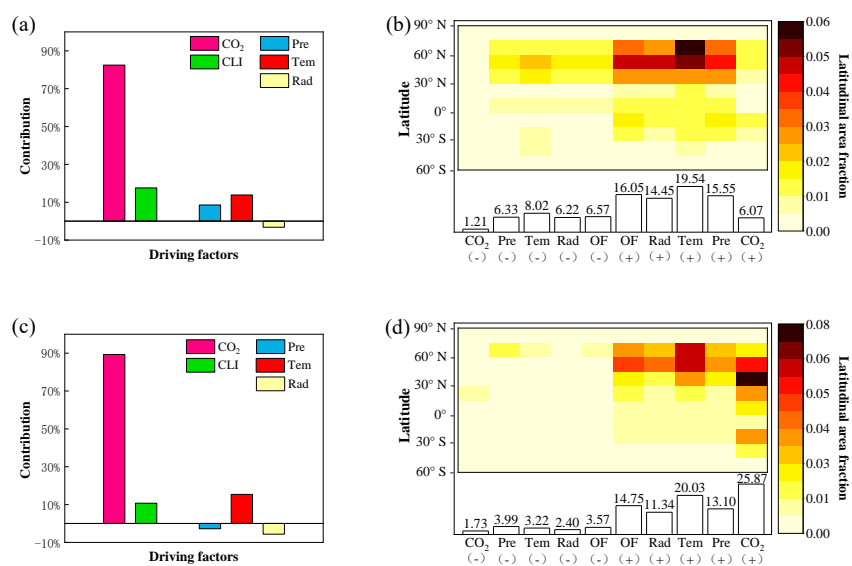
403 (Yang et al., 2010).

Figure 7. The proportion of change in the integrated vegetation biomass carbon stocks attributed to driving factors. Ratios of the driving factors of CO_2 fertilization effects (CO_2), climate change effects (CLI), precipitation (Pre), temperature (Tem), radiation (Rad) for AVBC (a) and

BVBC (c) under the five scenarios using the Mann-Kendall and Sen's slope estimator statistical tests. Attribution of AVBC (b) and BVBC (d) dynamics to driving factors calculated as averages along 15° latitude bands. At local scales, the driving factors include CO_2, Pre, Tem, Rad, and other climate factors (OF). A '+' symbol indicates a positive effect of the driving factor on carbon stock, and vice versa. The fraction of global area (%) that is predominantly influenced by the driving factors is shown at the top of the bar.

404 Climate change induced by the greenhouse effect explains part of the increase in carbon-stocks, but

405 unlike CO_2 fertilization, climate has dramatic negative effects on some vegetated regions. Figure 7

406 illustrates that temperature is the largest climatic contributor to the change in AVBC (13.83%, 2.572 g

407 m^{-2} yr^{-1}), followed by precipitation (8.51%, 1.572 g m^{-2} yr^{-1}) and radiation (–3.19%, –0.649 g m^{-2} yr^{-1}).

408 The spatial distribution shows that temperature predominantly influences the change in AVBC,

409 influencing over 27.56% of the global vegetated regions, followed by precipitation (21.88%) and

410 radiation (20.67%). Modelled BVBC trends based on the factorial simulations have similar

411 spatiotemporal patterns to AVBC. The effects of temperature on BVBC are stronger than AVBC, because

412 fine root tightly correlates with temperature (Gill, 2000). Meanwhile, there is a difference in the negative

413 contribution of precipitation to the change in BVBC at the global level (–2.76%, –0.013 g m^{-2} yr^{-1}). It

414 should be noted that trends in the global carbon-stock can be largely attributed to the influences of CO_2,

415 precipitation, temperature, and radiation (Figures 8, 9). Nonetheless, at the regional scale, the

416 contributions of other factors should be considered, such as humidity and wind speed. The effects of

417 these other factors dominate trends in AVBC in over 16.05% of the regions that increased and 6.57% of

418 the regions that decreased. In the case of changes in BVBC, other factors were dominant drivers in over

419 14.75% of the regions that increased and 3.57% of regions that decreased. Previous studies have pointed

420 out that the interannual variation of the terrestrial carbon-stock caused by releasing or sequestering

421 carbon is sensitive to anomalous changes in water availability and light use efficiency (Madani et al.,

422 2020; Humphrey et al., 2018). However, multidecade observational data revealed that there was not a

423 dramatic and consistent variant in the land surface precipitation and radiation data series (Sun et al., 2012;

424 Wild et al., 2005). It appears that the influences of precipitation and radiation on short-term variations in

425 the carbon-stocks were temporally compensated for by offsetting changes of AVBC, BVBC, and

426 AVBC/BVBC in the long-term trend. The accumulated influence of climate warming induces dramatic

427 changes in the carbon-stock at a global scale. Thus, we suggest that temperature dominates the long-term

428 trends in the carbon-stock among climatic drivers, while a compensatory effect exists in the long-term

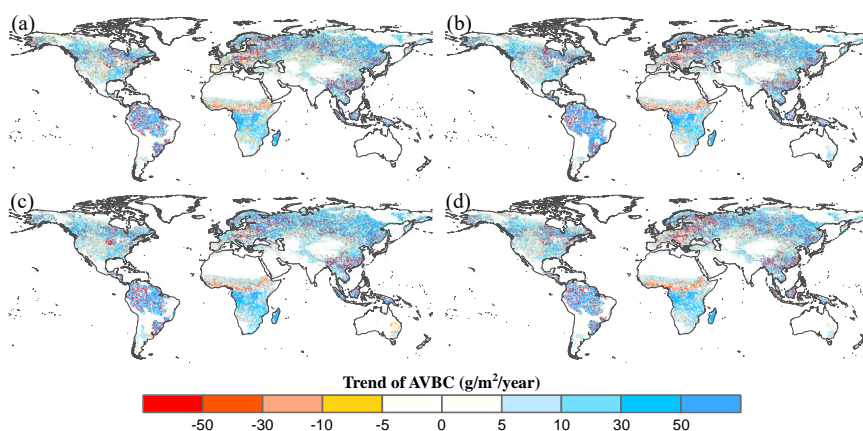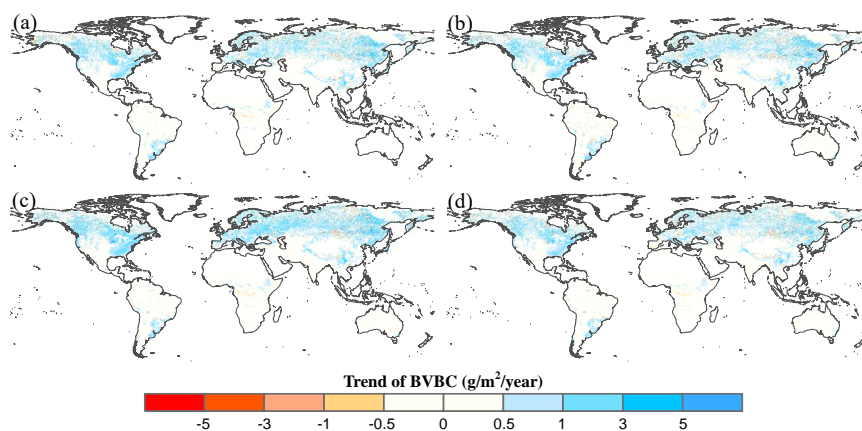429   change in the carbon-stock induced by precipitation and radiation.

Figure 8. Potential AVBC trend maps during the period of 1916 to 2015 under different factorial simulations. (a) CO_2 driving factorial simulation; (b) CO_2+precipitation driving factorial simulation. (c) CO_2+temperature driving factorial simulation; and (d) CO_2+radiation driving factorial simulation. Positive values indicate increasing trends in the ratio and vice versa. All results from Mann-Kendall and Sen's slope statistical tests correspond to the 95% confidence interval.

430

Figure 9. Potential BVBC variation trend maps during the period of 1916 to 2015 under different factorial simulations. (a) CO2 driving factorial simulation; (b) CO2+precipitation driving factorial simulation. (c) CO2+temperature driving factorial simulation; and (d) CO2+radiation driving factorial simulation. Positive values indicate increasing trends in the ratio and vice versa. All results from Mann-Kendall and Sen's slope statistical tests correspond to the 95% confidence interval.
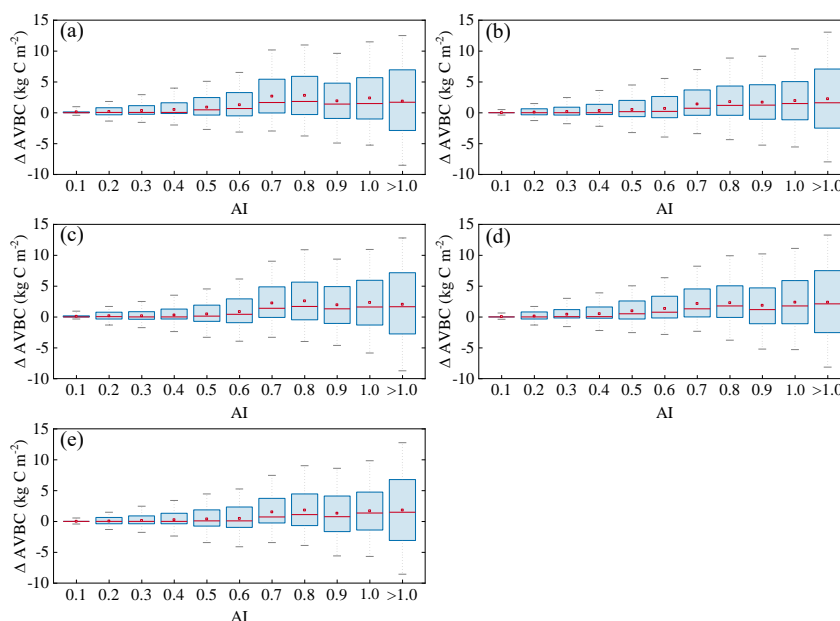
3.5 Constraints imposed by water limitations

Figure 10. Relationships in the incremental change between AI and AVBC over the hydrological regions. Modelled AVBC enhanced magnitude in the historical scenario S1 (a), CO_2 in scenario S2 (b), precipitation in scenario S3 (c), temperature in scenario S4 (d), and radiation in scenario S5 (e). Range of the box is 25%-75% of values; range of the whiskers is 10%-90% of values; the small red square is average value; and the red line is the median line.

Terrestrial water availability emerged as a key regulator of terrestrial carbon storage, by affecting the response mechanism of the vegetation carbon-stock to changes in driving factors (Fan et al., 2019; Humphrey et al., 2018; Ahlstrom et al., 2015; Madani et al., 2020; Humphrey et al., 2021; Ma et al., 2021). As shown in Figure 10, with an increase in the aridity index (i.e., an increase in available water), there is a gradually ascending trend in the enhanced magnitude and range in variation of AVBC density. Moreover, there is a link between fluctuations in the enhanced magnitude and range of variation in the BVBC density with the water stress gradient (Figure 11). These results suggest that water limitations lessen or even prevent carbon-stock fluctuations induced by changes in climate and CO_2. To further investigate the controls of water limitation on the responses of inner carbon storages to each driver, we analyse the long-term variability of potential vegetation carbon-stocks by means of factorial simulations for each hydrological region (Figure 1). In factorial simulations, drivers attributed to increase AVBC density changed from 0.878 ± 0.131 kg C m^{-2} in the hyper-arid regions to 5.459 ± 0.610 kg C m^{-2} in the

444   humid region during the past hundred years. Drivers attributed to increase BVBC density changed from

445   0.011 ± 0.001 kg C m^{-2} in the hyper-arid regions to 0.044 ± 0.005 kg C m^{-2} in the humid regions during

446   the same period (Figures A3, A4). With a lessening of water stress (from hyper-arid to humid area), the

447   response of the carbon-stock to changes in climate and CO_2 gradually became more noticeable. The

448   robust pattern in the regional average density of the carbon-stock shows that terrestrial water limitations

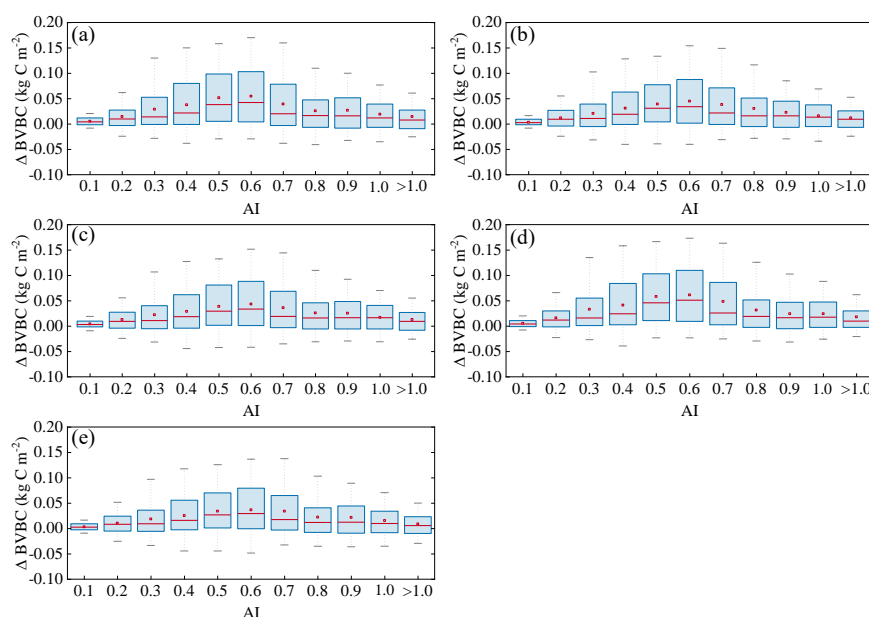449   strongly limit the enhanced magnitude of the carbon-stock.

Figure 11. Relationships in the incremental change in AI and BVBC over the hydrological regions. Modelled BVBC enhanced magnitude in the historical scenario S1 (a), CO_2 in scenario S2 (b), precipitation in scenario S3 (c), temperature in scenario S4 (d), and radiation in scenario S5 (e). Range of the box is 25%-75% of values; range of the whiskers is 10%-90% of values; the small red square is average value; and the red line is the median line.

450   Water limitations not only directly reduced the magnitude of the increase in the two fractions' carbon-

451   stock (AVBC and BVBC) to changes in climate and CO_2, but also indirectly confined the response

452   direction of each fractions' carbon-stock by transforming vegetation structure and function. Figure 12

453   illustrates that spatial variations in the carbon-stock ratio within and between hydrological regions. Under

454   the synergistic effect of drivers and water stress, vegetation carbon-stock increases, and there is a larger

455   proportion of biomass allocated to, and stored in, aboveground vegetation organs. In drylands (AI ≤ 0.5)

456   of all factorial simulations, aboveground and belowground biomass carbon-stocks both increased but the

457   rate of change in the AVBC/BVBC ratio gradually decreased. Vegetation utilizes a tolerance strategy to

458   allocate biomass, storing more biomass carbon in roots to resist enhanced water stress (Chen et al., 2013).

459   In humid regions (AI>0.65), the proportion of AVBC increases more than that of BVBC to obtain more

460   resources like CO_2 and radiation energy, leading to an increase in the AVBC/BVBC ratio. Conforming to

461   the optimal partitioning hypothesis, plants store more carbon in shoots and leaves in environments where

462   water is more available and shift more carbon to roots when water is more limited (Yang et al., 2010;

463   Mcconnaughay and Coleman, 1999). Terrestrial water availability has a strong regulating effect on the

464   spatial pattern of growth in the carbon-stock, demonstrating that the effects of the changes in climate and

465   CO_2 on the dynamics of the vegetation carbon-stock are controlled by the terrestrial water gradient.
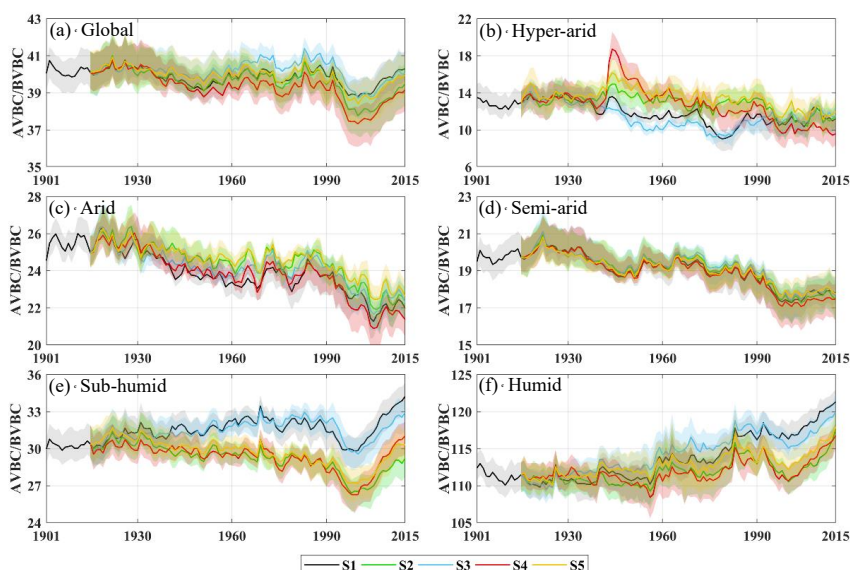

Figure 12. Temporal fluctuations in carbon-stock dynamics in vegetation biomass in different factorial simulations. Black indicates historical factorial simulation from 1901-2015, green indicates the CO_2-driven factorial simulation, blue indicates the precipitation-driven factorial simulation, red indicates the temperature-driving factorial simulation and yellow indicates radiation driven factorial simulation. Uncertainty bounds are provided as shaded areas reflect the intra-annual fluctuation (± 1 s.d.) **(a)** Modelled trend of AVBC/BVBC ratio in Global area. **(b-f)** Modelled trend of the AVBC/BVBC ratio in different hydrological regions.

466   **4 Conclusions and discussions**

467   To understand the response of carbon-sequestration potential and its inner biomass carbon-stocks to

468   environmental change, we conducted a series of factorial simulations using SEIB-DGVM V3.02. More

469   importantly, we investigated the extent of the responses of carbon-stocks to water limitations, and the

470   correlation between terrestrial water and carbon flux.

471

472   Over the past 100 years, there has been an ongoing increase in the carbon storage capacity of the

473   terrestrial ecosystem, which has slowed the rate at which atmospheric CO_2 has increased and may have

474   mitigated global warming. These findings are consistent with the conclusions of research conducted at

475   the local scale. For example, based on carbon flux data, Erb et al. (2008) suggested that the vegetation

476   carbon-stock in Austria increased from 1043 Mt C to 1249 Mt C (AVBC growth was 1.059 Mt C yr^{-1} and

477   BVBC growth was 0.2 Mt C yr^{-1}) since industrialization. Le Noë et al. (2020) showed that increases in

478   the carbon stocks and carbon density were the predominant drivers in the forest terrestrial carbon

479   sequestration capacity in France from 1850 to 2015. Tong et al. (2020) also found a substantial increase

480   of AVBC in southern China (0.11 Pg C yr^{-1}) during the period 2002–2017. However, these studies

481   focused on regional trends in integral vegetation carbon-stocks and did not investigate the extent of the

482   response in vegetation carbon-stocks partitioned between above- and belowground biomass. Our results

483   show that the increase in carbon-stock in aboveground vegetation was much larger than that in

484   belowground vegetation, and AVBC dominates the historical trend of the terrestrial carbon-stock. During

485   the past decades, the global land surface has been greening because of the flux and storage of more carbon

486   into plant trunks and foliage (Zhu et al., 2016). Based on our factorial simulations, the vegetation carbon-

487   stock exhibited the most increase under the combined influence of CO_2 fertilization and temperature. In

488   addition, the responses of carbon-stocks to other factors of change differed, particularly at the regional

489   scale (Figure 7). Temporal AVBC and BVBC variations driven by precipitation and radiation were

490   ultimately offset by compensatory effects, which dampened the long-term response of the carbon-stock

491   to these factors. Our results revealed that trends in CO_2 and temperature drove historical long-term trends

492   in the potential carbon-stocks, with faster increases and considerable variation occurring by region.

493

494   By partitioning the trends of AVBC and BVBC into five hydrological regions (Figure 1), we found that

495   the long-term change in carbon-stocks is tightly coupled to terrestrial water availability. These results

496   indicate that vegetation in humid regions is responsible for most of the trend in global AVBC, while

497   plants in semi-arid regions play a dominate global role in controlling the long-term trend in BVBC. In

498   addition, we demonstrated that water limitations controlled the terrestrial vegetation carbon-stocks (Ma

499   et al., 2021). As water stress decreases, the magnitude and range in variation of carbon-stocks gradually

500   increase (Figures 10, 11), which suggests that limited water availability constrains the response

501   magnitude of the changes in carbon-stocks to changes in CO_2 and climate. In contrast, we found that

502   indirect factors constrain the impact of increasing water stress on the response of carbon-stocks. Although

503   vegetation carbon-stocks dramatically increase under the effects of climate and CO_2 changes, vegetation

504   in humid regions stores more biomass (and carbon) in aboveground plant organs (trunk and foliage) to

505   obtain nutrients and light. Dryland vegetation lowers the AVBC/BVBC ratios and stores more biomass

506   below ground to enhance the capture of water resources. Terrestrial ecosystems utilize sensitive strategies

507   to allocate and store biomass to adjust to local hydrological conditions, which is consistent with optimal

508   partitioning theory (Mcconnaughay and Coleman, 1999). A significant conclusion is that water

509   constraints not only confine the responses of vegetation carbon-stocks to drivers of variability, but also

510   constrain the proportion of biomass carbon-stocks in above- and belowground fractions.

511

512   Distinguishing the response of carbon-stock fractions estimated by SEIB-DGVM improves the

513   understanding of the interactive impacts of terrestrial carbon and water dynamics. However, uncertainty

514   still exists because of the limitations in the processes of modelling vegetation metabolism with SEIB-

515   DGVM. Trunk biomass contains tree branches and structural roots (coarse roots and tap roots) (Sato et

516   al., 2007), so the R/S ratio of potential vegetation is smaller than the R/S of actual vegetation in factorial

517   simulations. Fine root biomass is just a tiny fraction to the total biomass, but is has a very high turnover

518   rate and determines the capacity of vegetation to absorb soil water. Availability of nitrogen is a key

519   limiting factor for vegetation growth, especially when higher CO_2 fertilization effects exist (Tharammal

520   et al., 2019). The limitation could be alleviated by nitrogen deposition in most temperate and boreal

521   ecosystems. The SEIB-DGVM experiments were conducted with a focus on documenting CO_2

522   fertilization and climate change interactions; these experiments did not consider the influences of

523   nitrogen deposition, which leads to a slight overestimate of the contributions of CO_2 fertilization on

524   biomass production.

525

526   In summary, we evaluated SEIB-DGVM V3.02 and used this model to offer new perspectives on the

527   response of vegetation carbon-sequestration potential to changes in climate and CO_2. Our simulation

528   results show that changes in CO_2, rather than climate, dominate the above to belowground partitioning

529   of the carbon-sequestration potential. More importantly, we suggest that the impact of CO_2 fertilization

530   and temperature effects on vegetation carbon-sequestration potential depends on water availability and

531   its impacts on plant stress. With increased global warming, water limitations are expected to increasingly

532   confine global carbon-sequestration. Our findings highlight the need to account for terrestrial water

533   limitation effects when estimating the response of the terrestrial carbon sequestration capacity to global

534   climate change, and the need for stronger interactions between those involved in vegetation model

535   development and those in between the hydrological and ecological research communities.
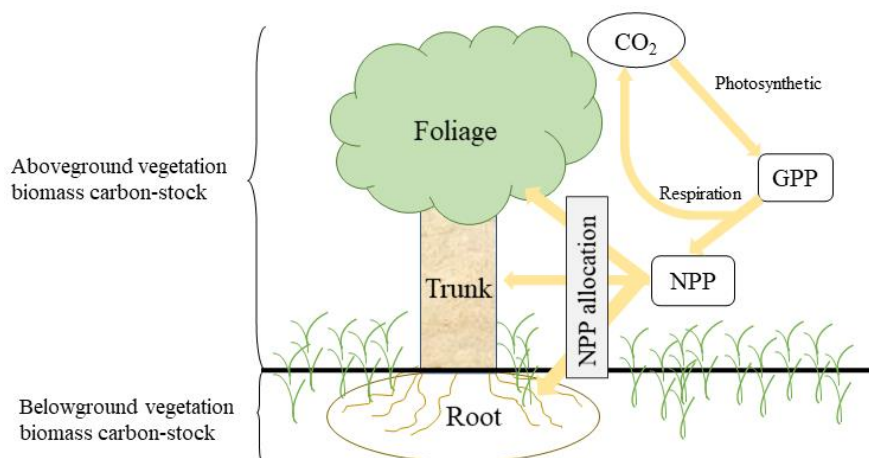
Appendices

Figure A1. Schematic of ecosystem carbon cycle. Yellow arrow indicates carbon flux. Atmospheric CO_2 transitions into gross primary production (GPP) by photosynthesis. GPP is partitioned into respiration and net primary production (NPP). NPP is partitioned into three biomass carbon pools (foliage, trunk, and root).
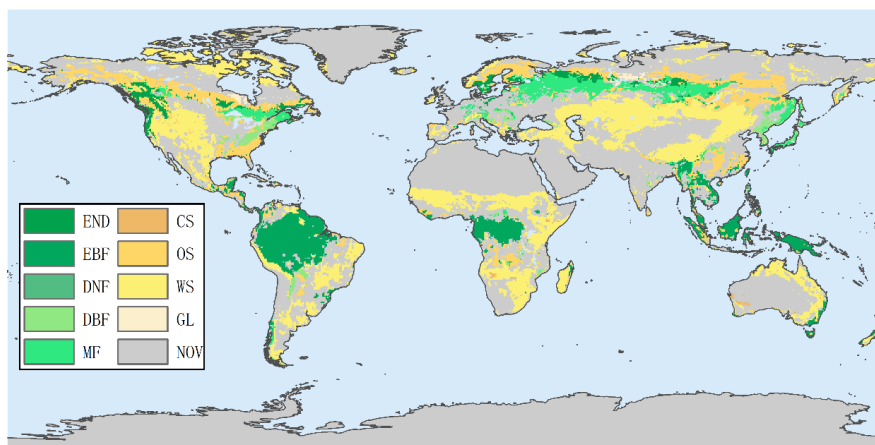

Figure A2. Land vegetation cover map from MCD12C1. END: Evergreen needleleaf forest, EBF: Evergreen broadleaf forest, DNF: Deciduous needleleaf forest, DBF: Deciduous broadleaf forest, MF: Mixed forest, CS: Closed shrublands, OS: Open shrublands, WS: Woody savannas, GL: Grasslands, NOV: No value.
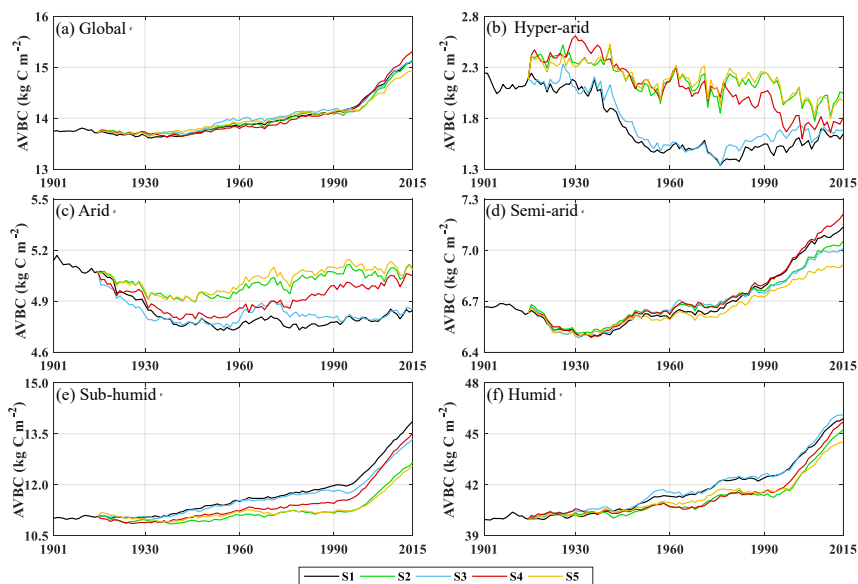
Figure A3. Trends in average density of potential AVBC. (a) Modelled trend of annual averaged BVBC globally. Modelled trends in annual averaged AVBC in hyper-arid regions (b), arid regions (c), semi-arid regions (d), sub-humid regions (e), and humid regions (f).
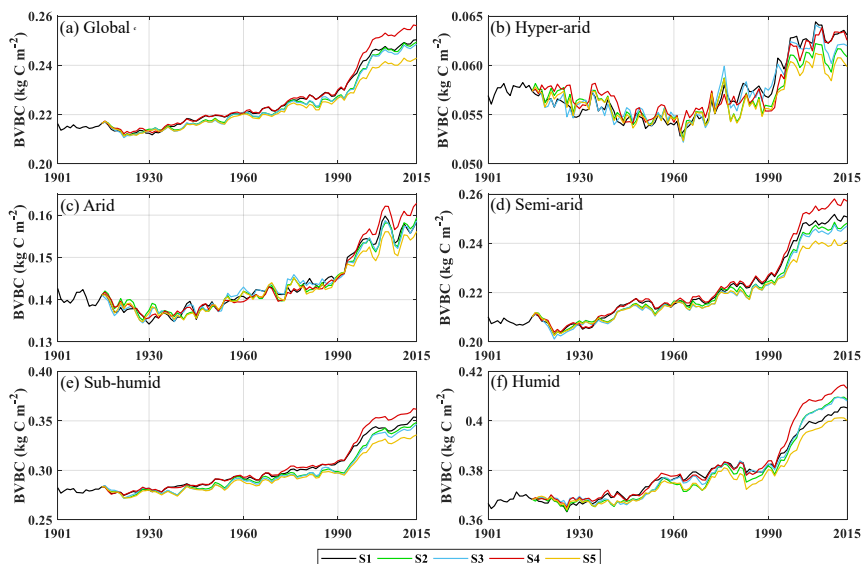
539

Figure A4. Trends in average density of potential BVBC. (a) Modelled trend of annual averaged BVBC globally. Modelled trends in annual averaged BVBC in hyper-arid regions (b), arid regions (c),

semi-arid regions (d), sub-humid regions (e), and humid regions (f).

Code and data availability statement

The code of SEIB-DGVM version 3.02 can be download from http://seib-dgvm.com/. Climatic Research Unit data can be downloaded from https://crudata.uea.ac.uk/cru/data/hrg/. The soil physical parameters can be downloaded from www.iges.org/gswp. The reconstructed CO_2 concentration dataset and SEIB code can be downloaded from http://seib-dgvm.com/. In model validation, Ecosystem Model-Data Intercomparison (multiyear average NPP product) data were collected from https://daac.ornl.gov/NPP/guides/NPP_EMDI.html. Remote sensing product MOD17A3 data were obtained from https://lpdaac.usgs.gov/products/mod17a3hgfv006/, and MCD12C1 data were obtained from https://ladsweb.modaps.eosdis.nasa.gov/search/order.

Authors contributions

T.S. designed research. T.S., and S.H. performed research and developed the methodology. T.S. analyzed data and produced the outputs. T.S., S.H., C.J., and X.C. wrote the first manuscript draft. W.W. and W.G. supervised the study. All the authors discussed the methodology and commented on various versions of the manuscript.

Competing interests

The authors declare that they have no conflict of interest.

Acknowledgments

564   the Center for Ocean-Land-Atmosphere Studies (COLA).

References

565 **References**

566 Ahlstrom, A., Raupach, M. R., Schurgers, G., Smith, B., Arneth, A., Jung, M., Reichstein, M., Canadell,
567   J. G., Friedlingstein, P., Jain, A. K., Kato, E., Poulter, B., Sitch, S., Stocker, B. D., Viovy, N., Wang,
568   Y. P., Wiltshire, A., Zaehle, S., and Zeng, N.: The dominant role of semi-arid ecosystems in the
569   trend and variability of the land CO2 sink, Science, 348, 895-899, 10.1126/science.aaa1668, 2015.

570 Ajtay, G. L., Ketner, P., and Duvigneaud, P.: Terrestrial primary production and phytomass In: The Global
571   Cycle., Glob. Carbon Cycle, SCOPE, 129-181 pp.1979.

572 Anderson, L. J., Derner, J. D., Polley, H. W., Gordon, W. S., Eissenstat, D. M., and Jackson, R. B.: Root
573   responses along a subambient to elevated CO2 gradient in a C3-C4 grassland, Global Change Biol,
574   16, 454-468, 10.1111/j.1365-2486.2009.01975.x, 2010.

575 Bartholome, E. and Belward, A. S.: GLC2000: a new approach to global land cover mapping from Earth
576   observation data, Int J Remote Sens, 26, 1959-1977, 10.1080/01431160412331291297, 2005.

577 Bayer, A. D., Pugh, T. A. M., Krause, A., and Arneth, A.: Historical and future quantification of terrestrial
578   carbon sequestration from a Greenhouse-Gas-Value perspective, Global Environmental Change, 32,
579   153-164, 10.1016/j.gloenvcha.2015.03.004, 2015.

580 Bazilevich, N. I., Rodin, L. Y., and Rozov, N. N.: Geographical Aspects of Biological Productivity, Soviet
581   Geograpgy Review and Translation, 5, 293-317 pp.1971.

582 Bloom, A. A., Exbrayat, J. F., van der Velde, I. R., Feng, L., and Williams, M.: The decadal state of the
583   terrestrial carbon cycle: Global retrievals of terrestrial carbon allocation, pools, and residence times,
584   Proceedings of the National Academy of Sciences of the United States of America, 113, 1285-1290,
585   10.1073/pnas.1515160113, 2016.

586 Chen, J., Ju, W., Ciais, P., Viovy, N., Liu, R. G., Liu, Y., and Lu, X. H.: Vegetation structural change since
587   1981 significantly enhanced the terrestrial carbon sink, Nat Commun, 10, 4259, 10.1038/S41467-
588   019-12257-8, 2019.

589 Chen, L.-P., Zhao, N.-X., Zhang, L.-H., and Gao, Y.-B.: Responses of two dominant plant species to
590   drought stress and defoliation in the Inner Mongolia Steppe of China, Plant Ecology, 214, 221-229,
591   10.1007/s11258-012-0161-y, 2013.

592 Cheng, L., Zhang, L., Wang, Y. P., Canadell, J. G., Chiew, F. H. S., Beringer, J., Li, L. H., Miralles, D.
593   G., Piao, S. L., and Zhang, Y. Q.: Recent increases in terrestrial carbon uptake at little cost to the
594   water cycle, Nat Commun, 8, 10.1038/s41467-017-00114-5, 2017.

595 Erb, K.-H., Gingrich, S., Krausmann, F., and Haberl, H.: Industrialization, Fossil Fuels, and the
596   Transformation of Land Use, Journal of Industrial Ecology, 12, 686-703, 10.1111/j.1530-
597   9290.2008.00076.x, 2008.

598 Erb, K.-H., Gaube, V., Krausmann, F., Plutzar, C., Bondeau, A., and Haberl, H.: A comprehensive global
599   5min resolution land-use data set for the year 2000 consistent with national census data, Journal of
600   Land Use Science, 2, 191-224, 10.1080/17474230701622981, 2007.

601 Erb, K.-H., Fetzel, T., Plutzar, C., Kastner, T., Lauk, C., Mayer, A., Niedertscheider, M., Körner, C., and
602   Haberl, H.: Biomass turnover time in terrestrial ecosystems halved by land use, Nat Geosci, 9, 674-
603   678, 10.1038/ngeo2782, 2016.

604 Erb, K.-H., Kastner, T., Plutzar, C., Bais, A. L. S., Carvalhais, N., Fetzel, T., Gingrich, S., Haberl, H.,
605   Lauk, C., Niedertscheider, M., Pongratz, J., Thurner, M., and Luyssaert, S.: Unexpectedly large
606   impact of forest management and grazing on global vegetation biomass, Nature, 553, 73-76,
607   10.1038/nature25138, 2018.

608   Fan, L., Wigneron, J. P., Ciais, P., Chave, J., Brandt, M., Fensholt, R., Saatchi, S. S., Bastos, A., Al-Yaari,
609   A., Hufkens, K., Qin, Y. W., Xiao, X. M., Chen, C., Myneni, R. B., Fernandez-Moran, R., Mialon,
610   A., Rodriguez-Fernandez, N. J., Kerr, Y., Tian, F., and Penuelas, J.: Satellite-observed pantropical
611   carbon dynamics, Nat Plants, 5, 944-951, 10.1038/s41477-019-0478-9, 2019.

612   Fang, J., Yang, Y., Ma, W., Mohammat, A., and Shen, H.: Ecosystem carbon stocks and their changes in
613   China's grasslands, Science China. Life sciences, 53, 757-765, 10.1007/s11427-010-4029-x, 2010.

614   Friedlingstein, P., Joel, G., Field, C. B., and Fung, I. Y.: Toward an allocation scheme for global terrestrial
615   carbon models, Global Change Biol, 5, 755-770, DOI 10.1046/j.1365-2486.1999.00269.x, 1999.

616   Gentine, P., Green, J. K., Guérin, M., Humphrey, V., Seneviratne, S. I., Zhang, Y., and Zhou, S.: Coupling
617   between the terrestrial carbon and water cycles—a review, Environ Res Lett, 14, 083003,
618   10.1088/1748-9326/ab22d6, 2019.

619   Gill, R.: Global patterns of root turnover for terrestrial ecosystems, New Phytol, 147, 13-31, 2000.

620   Gocic, M. and Trajkovic, S.: Analysis of changes in meteorological variables using Mann-Kendall and
621   Sen's slope estimator statistical tests in Serbia, Global and Planetary Change, 100, 172-182,
622   10.1016/j.gloplacha.2012.10.014, 2013.

623   Gulbeyaz, O., Bond-Lamberty, B., Akyurek, Z., and West, T. O.: A new approach to evaluate the MODIS
624   annual NPP product (MOD17A3) using forest field data from Turkey, Int J Remote Sens, 39, 2560-
625   2578, 10.1080/01431161.2018.1430913, 2018.

626   Haberl, H., Erb, K. H., and Krausmann, F.: Human Appropriation of Net Primary Production: Patterns,
627   Trends, and Planetary Boundaries, Annu Rev Env Resour, 39, 363-391, 10.1146/annurev-environ-
628   121912-094620, 2014.

629   Harper, A. B., Wiltshire, A. J., Cox, P. M., Friedlingstein, P., Jones, C. D., Mercado, L. M., Sitch, S.,
630   Williams, K., and Duran-Rojas, C.: Vegetation distribution and terrestrial carbon cycle in a carbon
631   cycle configuration of JULES4.6 with new plant functional types, Geosci Model Dev, 11, 2857-
632   2873, 10.5194/gmd-11-2857-2018, 2018.

633   Harris, I., Osborn, T. J., Jones, P., and Lister, D.: Version 4 of the CRU TS monthly high-resolution
634   gridded multivariate climate dataset, Scientific Data, 7, 109, 10.1038/s41597-020-0453-3, 2020.

635   Hovenden, M. J., Newton, P. C., and Wills, K. E.: Seasonal not annual rainfall determines grassland
636   biomass response to carbon dioxide, Nature, 511, 583-586, 10.1038/nature13281, 2014.

637   Humphrey, V., Zscheischler, J., Ciais, P., Gudmundsson, L., Sitch, S., and Seneviratne, S. I.: Sensitivity
638   of atmospheric CO2 growth rate to observed changes in terrestrial water storage, Nature, 560, 628-
639   631, 10.1038/s41586-018-0424-4, 2018.

640   Humphrey, V., Berg, A., Ciais, P., Gentine, P., Jung, M., Reichstein, M., Seneviratne, S. I., and
641   Frankenberg, C.: Soil moisture–atmosphere feedback dominates land carbon uptake variability,
642   Nature, 592, 65-69, 10.1038/s41586-021-03325-5, 2021.

643   Hurtt, G. C., Chini, L. P., Frolking, S., Betts, R. A., Feddema, J., Fischer, G., Fisk, J. P., Hibbard, K.,
644   Houghton, R. A., Janetos, A., Jones, C. D., Kindermann, G., Kinoshita, T., Goldewijk, K. K., Riahi,
645   K., Shevliakova, E., Smith, S., Stehfest, E., Thomson, A., Thornton, P., van Vuuren, D. P., and Wang,
646   Y. P.: Harmonization of land-use scenarios for the period 1500-2100: 600 years of global gridded
647   annual land-use transitions, wood harvest, and resulting secondary lands, Climate Change, 109, 117-
648   161, 10.1007/s10584-011-0153-2, 2011.

649   IPCC: Impacts, Adaptation and Vulnerability. Contribution of Working Group II to the Fourth
650   Assessment Report of the Intergovernmental Panel on Climate Change, 2007.

651   Jung, M., Reichstein, M., Schwalm, C. R., Huntingford, C., Sitch, S., Ahlstrom, A., Arneth, A., Camps-

652 Valls, G., Ciais, P., Friedlingstein, P., Gans, F., Ichii, K., Jain, A. K., Kato, E., Papale, D., Poulter,
653 B., Raduly, B., Rodenbeck, C., Tramontana, G., Viovy, N., Wang, Y. P., Weber, U., Zaehle, S., and
654 Zeng, N.: Compensatory water effects link yearly global land CO_2 sink changes to temperature,
655 Nature, 541, 516-520, 10.1038/nature20780, 2017.

656 Kaplan, J. O., Krumhardt, K. M., Ellis, E. C., Ruddiman, W. F., Lemmen, C., and Goldewijk, K. K.:
657 Holocene carbon emissions as a result of anthropogenic land cover change, Holocene, 21, 775-791,
658 10.1177/0959683610386983, 2011.

659 Keenan, T. F., Prentice, I. C., Canadell, J. G., Williams, C. A., Wang, H., Raupach, M., and Collatz, G.
660 J.: Recent pause in the growth rate of atmospheric CO_2 due to enhanced terrestrial carbon uptake
661 Nat Commun, 7, 10.1038/Ncomms16137, 2017.

662 Kindermann, G. E., Mcallum, I., Fritz, S., and Obersteiner, M.: A global forest growing stock, biomass
663 and carbon map based on FAO statistics, Silva Fenn, 42, 387-396, 10.14214/Sf.244, 2008.

664 Le Noë, J., Matej, S., Magerl, A., Bhan, M., Erb, K. H., and Gingrich, S.: Modeling and empirical
665 validation of long-term carbon sequestration in forests (France, 1850-2015), Glob Chang Biol, 26,
666 2421-2434, 10.1111/gcb.15004, 2020.

667 Liu, J., Bowman, K. W., Schimel, D. S., Parazoo, N. C., Jiang, Z., Lee, M., Bloom, A. A., Wunch, D.,
668 Frankenberg, C., Sun, Y., O'Dell, C. W., Gurney, K. R., Menemenlis, D., Gierach, M., Crisp, D., and
669 Eldering, A.: Contrasting carbon cycle responses of the tropical continents to the 2015-2016 El Nino,
670 Science, 358, eaam5690, 10.1126/science.aam5690, 2017.

671 Ma, H. Z., Mo, L. D., Crowther, T. W., Maynard, D. S., van den Hoogen, J., Stocker, B. D., Terrer, C.,
672 and Zohner, C. M.: The global distribution and environmental drivers of aboveground versus
673 belowground plant biomass, Nat Ecol Evol, 5, 1110-+, 10.1038/s41559-021-01485-1, 2021.

674 Madani, N., Parazoo, N. C., Kimball, J. S., Ballantyne, A. P., Reichle, R. H., Maneta, M., Saatchi, S.,
675 Palmer, P. I., Liu, Z., and Tagesson, T.: Recent Amplified Global Gross Primary Productivity Due
676 to Temperature Increase Is Offset by Reduced Productivity Due to Water Constraints, AGU
677 Advances, 2, e2020AV000180, 10.1029/2020AV000180, 2020.

678 Magerl, A., Le Noë, J., Erb, K.-H., Bhan, M., and Gingrich, S.: A comprehensive data-based assessment
679 of forest ecosystem carbon stocks in the U.S. 1907–2012, Environ Res Lett, 14, 125015,
680 10.1088/1748-9326/ab5cb6, 2019.

681 McConnaughay, K. D. M. and Coleman, J. S.: Biomass allocation in plants: ontogeny or optimality? A
682 test along three resource gradients, Ecology, 80, 2581-2593, 10.1890/0012-
683 9658(1999)080[2581:BAIPOO]2.0.CO;2, 1999.

684 Monteith, J. L. and Unsworth, M. H.: Principles of Environmental Physics, 2nd ed., London1990.

685 Olson, J., Watts, J., and Allison, L.: Carbon in Live Vegetation of Major World Ecosystems, Oak Ridge
686 National Laboratory1983.

687 Pan, Y. D., Birdsey, R. A., Phillips, O. L., and Jackson, R. B.: The Structure, Distribution, and Biomass
688 of the World's Forests, Annu Rev Ecol Evol S, 44, 593-622, 10.1146/annurev-ecolsys-110512-
689 135914, 2013.

690 Pan, Y. D., Birdsey, R. A., Fang, J. Y., Houghton, R., Kauppi, P. E., Kurz, W. A., Phillips, O. L., Shvidenko,
691 A., Lewis, S. L., Canadell, J. G., Ciais, P., Jackson, R. B., Pacala, S. W., McGuire, A. D., Piao, S.
692 L., Rautiainen, A., Sitch, S., and Hayes, D.: A Large and Persistent Carbon Sink in the World's
693 Forests, Science, 333, 988-993, 10.1126/science.1201609, 2011.

694 Piao, S. L., Friedlingstein, P., Ciais, P., Zhou, L. M., and Chen, A. P.: Effect of climate and CO_2 changes
695 on the greening of the Northern Hemisphere over the past two decades, Geophys Res Lett, 33,

696   L23402, 10.1029/2006GL028205, 2006.

697 Piao, S. L., Wang, X., Wang, K., Li, X., Bastos, A., Canadell, J. G., Ciais, P., Friedlingstein, P., and Sitch,
698   S.: Interannual variation of terrestrial carbon cycle: Issues and perspectives, Glob Chang Biol, 26,
699   300-318, 10.1111/gcb.14884, 2020.

700 Poorter, H.: Construction costs and payback time of biomass: a whole plant perspective, A Whole-Plant
701   Perspective on Carbon-Nitrogen Interactions, SPB Academic Publishing, The Hague1994.

702 Poulter, B., Frank, D., Ciais, P., Myneni, R. B., Andela, N., Bi, J., Broquet, G., Canadell, J. G., Chevallier,
703   F., Liu, Y. Y., Running, S. W., Sitch, S., and van der Werf, G. R.: Contribution of semi-arid
704   ecosystems to interannual variability of the global carbon cycle, Nature, 509, 600-603,
705   10.1038/nature13376, 2014.

706 Prentice, I. C., Harrison, S. P., and Bartlein, P. J.: Global vegetation and terrestrial carbon cycle changes
707   after the last ice age, New Phytol, 189, 988-998, 10.1111/j.1469-8137.2010.03620.x, 2011.

708 Roy, J., Saugier, B., and Mooney, H. A.: Estimations of global terrestrial productivity: converging toward
709   a single number? In: Terrestrial Global Productivity, Academic Press, San Diego2001.

710 Ruesch, A. and Gibbs, H. K.: New IPCC Tier-1 global biomass carbon map for the year 2000, 2008.

711 Ryan, M. G.: Effects of Climate Change on Plant Respiration, Ecological Applications, 1, 157-167,
712   10.2307/1941808, 1991.

713 Sato, H., Itoh, A., and Kohyama, T.: SEIB–DGVM: A new Dynamic Global Vegetation Model using a
714   spatially   explicit   individual-based   approach,   Ecological   Modelling,   200,   279-307,
715   10.1016/j.ecolmodel.2006.09.006, 2007.

716 Sato, H., Kobayashi, H., Beer, C., and Fedorov, A.: Simulating interactions between topography,
717   permafrost, and vegetation in Siberian larch forest, Environ Res Lett, 15, 095006, 10.1088/1748-
718   9326/Ab9be4, 2020.

719 Saugier, B., Roy, J., and Mooney, H.: Estimations of Global Terrestrial Productivity, Terrestrial Global
720   Productivity, Academic Press, San Diego, Calif2001.

721 Schimel, D., Stephens, B. B., and Fisher, J. B.: Effect of increasing CO2 on the terrestrial carbon cycle,
722   Proceedings of the National Academy of Sciences of the United States of America, 112, 436-441,
723   10.1073/pnas.1407302112, 2015.

724 Seo, H. and Kim, Y.: Interactive impacts of fire and vegetation dynamics on global carbon and water
725   budget using Community Land Model version 4.5, Geosci Model Dev, 12, 457-472, 10.5194/gmd-
726   12-457-2019, 2019.

727 Shevliakova, E., Pacala, S. W., Malyshev, S., Hurtt, G. C., Milly, P. C. D., Caspersen, J. P., Sentman, L.
728   T., Fisk, J. P., Wirth, C., and Crevoisier, C.: Carbon cycling under 300 years of land use change:
729   Importance of the secondary vegetation sink, Global Biogeochem Cy, 23, 10.1029/2007gb003176,
730   2009.

731 Sun, F., Roderick, M. L., and Farquhar, G. D.: Changes in the variability of global land precipitation,
732   Geophys Res Lett, 39, L19402, 10.1029/2012gl053369, 2012.

733 Tei, S., Sugimoto, A., Liang, M. C., Yonenobu, H., Matsuura, Y., Osawa, A., Sato, H., Fujinuma, J., and
734   Maximov, T.: Radial Growth and Physiological Response of Coniferous Trees to Arctic
735   Amplification, J Geophys Res-Biogeo, 122, 2786-2803, 10.1002/2016JG003745, 2017.

736 Terrer, C., Phillips, R. P., Hungate, B. A., Rosende, J., Pett-Ridge, J., Craig, M. E., van Groenigen, K. J.,
737   Keenan, T. F., Sulman, B. N., Stocker, B. D., Reich, P. B., Pellegrini, A. F. A., Pendall, E., Zhang,
738   H., Evans, R. D., Carrillo, Y., Fisher, J. B., Van Sundert, K., Vicca, S., and Jackson, R. B.: A trade-
739   off between plant and soil carbon storage under elevated CO2, Nature, 591, 599-603,

740　　　　10.1038/s41586-021-03306-8, 2021.

741　Tharammal, T., Bala, G., Devaraju, N., and Nemani, R.: A review of the major drivers of the terrestrial
742　　　　carbon uptake: model-based assessments, consensus, and uncertainties, Environ Res Lett, 14,
743　　　　093005, 10.1088/1748-9326/Ab3012, 2019.

744　Tong, X. W., Brandt, M., Yue, Y. M., Ciais, P., Jepsen, M. R., Penuelas, J., Wigneron, J. P., Xiao, X. M.,
745　　　　Song, X. P., Horion, S., Rasmussen, K., Saatchi, S., Fan, L., Wang, K. L., Zhang, B., Chen, Z. C.,
746　　　　Wang, Y. H., Li, X. J., and Fensholt, R.: Forest management in southern China generates short term
747　　　　extensive carbon sequestration, Nat Commun, 11, 10.1038/s41467-019-13798-8, 2020.

748　West, P. C., Gibbs, H. K., Monfreda, C., Wagner, J., Barford, C. C., Carpenter, S. R., and Foley, J. A.:
749　　　　Trading carbon for food: Global comparison of carbon stocks vs. crop yields on agricultural land,
750　　　　Proceedings of the National Academy of Sciences of the United States of America, 107, 19645-
751　　　　19648, 10.1073/pnas.1011078107, 2010.

752　Wild, M., Gilgen, H., Roesch, A., Ohmura, A., Long, C. N., Dutton, E. G., Forgan, B., Kallis, A., Russak,
753　　　　V., and Tsvetkov, A.: From dimming to brightening: Decadal changes in solar radiation at Earth's
754　　　　surface, Science, 308, 847-850, 10.1126/science.1103215, 2005.

755　Yang, Y., Fang, J., Ma, W., Guo, D., and Mohammat, A.: Large-scale pattern of biomass partitioning
756　　　　across China's grasslands, Global Ecology and Biogeography, 19, 268-277, 10.1111/j.1466-
757　　　　8238.2009.00502.x, 2010.

758　Zhang, H., Song, T. Q., Wang, K. L., Yang, H., Yue, Y. M., Zeng, Z. X., Peng, W. X., and Zeng, F. P.:
759　　　　Influences of stand characteristics and environmental factors on forest biomass and root-shoot
760　　　　allocation in southwest China, Ecol Eng, 91, 7-15, 10.1016/j.ecoleng.2016.01.040, 2016.

761　Zhu, Z. C., Piao, S. L., Myneni, R. B., Huang, M. T., Zeng, Z. Z., Canadell, J. G., Ciais, P., Sitch, S.,
762　　　　Friedlingstein, P., Arneth, A., Cao, C. X., Cheng, L., Kato, E., Koven, C., Li, Y., Lian, X., Liu, Y.
763　　　　W., Liu, R. G., Mao, J. F., Pan, Y. Z., Peng, S. S., Penuelas, J., Poulter, B., Pugh, T. A. M., Stocker,
764　　　　B. D., Viovy, N., Wang, X. H., Wang, Y. P., Xiao, Z. Q., Yang, H., Zaehle, S., and Zeng, N.: Greening
765　　　　of the Earth and its drivers, Nat Clim Change, 6, 791-+, 10.1038/Nclimate3004, 2016.

766